IEEE Access
Multidisciplinary | Rapid Review | Open Access Journal

Received March 25, 2022, accepted May 17, 2022, date of publication May 23, 2022, date of current version May 27, 2022.

Digital Object Identifier 10.1109/ACCESS.2022.3176850

SVM-Based Optimizing Control of Two-Phase Winding Segmented Permanent Magnet Linear Synchronous Motor

TUANSHAN ZHANG[1,2], XUESONG MEI[1], AND XIN DU[2]
[1]Mechanical Engineering Department, Xi'an Jiaotong University, Xi'an, Shaanxi 710049, China
[2]Mechanical and Electrical Engineering Department, Xi'an Polytechnic University, Xi'an, Shaanxi 710048, China

Corresponding author: Xuesong Mei (xsmei@mail.xjtu.edu.cn)

This work was supported in part by the Natural Science Foundation of China under Grant 51735010, and in part by the Xi'an Key Laboratory of Modern Intelligent Textile Equipment under Grant 2019220614SYS021CG043.

ABSTRACT This paper presents a space vector modulation (SVM) technique for a two-phase winding segmented permanent magnet linear synchronous motor (WS-PMLSM). First, the advantages of the two-phase WS-PMLSM are discussed, the parameters related to the WS-PMLSM mathematical model are analyzed, and the SVM is applied to the implementation of the WS-PMLSM two-phase sinusoidal voltage inverter. Next, a feedforward implementation method is proposed considering the regularity characteristics of the mover cross-zone operation. Finally, in order to improve the smoothness of operation, an optimal calculation of the current values of each section according to the coverage is proposed, and an optimal control method is implemented by establishing an optimal efficiency model. The experimental results prove the effectiveness of the proposed method.

INDEX TERMS Space vector modulation (SVM), two-phase linear synchronous motor, winding segmented permanent magnet linear synchronous motor (WS-PMLSM), mover operation across sections, optimal control method.

In modern factory automation lines or semiconductor production lines, many carriers carrying raw materials and semi-finished products are precisely servo-controlled along a track consisting of closed loops. Therefore, very long tracks, multiple vehicles traveling at high speeds, high positioning repeatability and the potential for fast acceleration make short primary linear drives good candidates for material transfer and processing lines, with which to precisely and individually control multiple passive carriers carrying materials and semi-finished products along a single closed track [1]. Fig. 1 shows an example for material handling and processing, where several movers (workpiece carriers) travel highly independently on the same track, four processing stations (P1-P4) are distributed along the track, and vehicles (V1-V4) move outside the processing stations [2].

In this construction, there is no need for power operating cables moving along the mover and the problem of heat dissipation is made easy by the fact that the coil through which the current flows is fixed to the track. In addition, since the unenergized carrier has no heating elements, it can be maintained at a constant temperature, which is helpful for temperature-sensitive processes, such as semiconductor or flat panel display manufacturing.

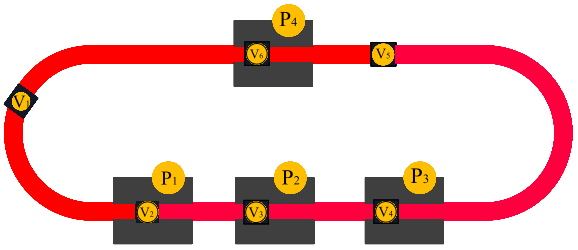

FIGURE 1. Simple example of the proposed linear drive system.

As a new type of linear motor, WS-PMLSM has the advantages of high thrust density, low power loss, and fast dynamic response. Many literatures have carried out in-depth research on the key technologies of this motor, such as segmented

The associate editor coordinating the review of this manuscript and approving it for publication was Zhuang Xu.

winding structure [3], electromagnetic properties [4], current control [5], segmented principle and method [6], Variant electromagnetic parameter law [7], drive circuit design and winding switching control method [8], internode thrust fluctuation suppression and non-inductive control [9]. In addition, some results have been obtained, such as predictive current control [10], capacitive position sensor [11], torque control (DTC) [12], transition inductance [13], etc.

Therefore, this paper proposes a novel WS-PMSLM motor structure using two-phase integer single-layer concentric distributed windings [14]. The motor consists of a segmented stator and a passive mover. The length of the passive mover is the same as that of the segmented stator or the same pole pitch. Fig. 2 shows the physical and coil diagram of the two-phase WS-PMLSM.

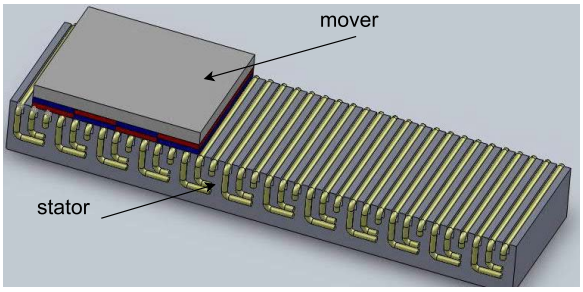

(a) Physical drawing of motor structure.

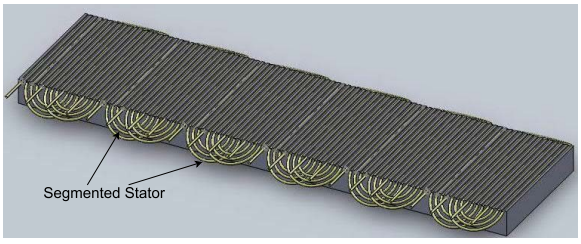

(b) Schematic of motor coil.

FIGURE 2. **Motor model.**

This type of motor has many advantages [15], including:

1) Two-phase motors are phase-balanced because the magnetic circuit for each phase is the same. Therefore, it eliminates the control problems associated with phase asymmetry prevalent in three-phase linear motors [16]. Thus, the motor can generate a position-invariant electromagnetic thrust and is easier to control.
2) The two windings of a two-phase motor are spatially perpendicular to each other, so there is no Clark and inverse Clark transformation, vector control is easy to implement, and the requirements for chip performance are not very high.
3) In single-layer windings, only one winding is embedded in each stator slot along the effective side of the coil, which results in fewer winding coils, a simpler process, and an increased slot fill rate. In addition, in the case of single-layer failure, there are no interlayer junctions and no phase breakdown. In addition, sinusoidal windings allow for improved concentric patterns and reduced harmonics.

WS-PMLSM is equivalent to multiple PMLSM spliced together, the electromagnetic parameters will change drastically when the mover operates across segments [17], if the stator current of each segment cannot be accurately coordinated and controlled will cause the output thrust of each segment of the stator to be unbalanced. This will cause thrust fluctuations [18] and even lead to the reverse thrust between the two stator segments canceling each other and reducing the output characteristics of the drive system. The coordination, speed and stability control of the stator currents in each segment will determine the whole control system. On the other hand, WS-PMLSM divides a linear synchronous motor stator into smaller sections for performance, manufacturability and maintenance purposes. A segmented stator system is fundamentally different from a single segmented stator system and requires compensation for optimal operation [19].

Therefore, this paper first analyzes the mathematical model of WS-PMLSM and its related parameter characteristics, and then considers the use of SVM to control a two-phase WS-PMLSM, proposes a full H-bridge inverter, and derives the corresponding optimal switching voltage vector table, two-phase space vector (SV) pulse width modulation (PWM) strategy [20], and its application in a vector control (VC) scheme. Finally, a method to optimize the efficiency of a multi-stator arrangement by using different currents in each active stator section is proposed, the consequences of the optimal efficiency method are discussed, and an implementation method with an optimal scheme is given.

I. MATHEMATICAL MODELS

Unlike conventional PMLSM, the structure of the magnetic circuit between the primary and secondary of SW-PMLSM varies with the relative position, so the electromagnetic (EM) parameters of the motor are a function of the secondary position. If the effect of magnetic saturation is taken into account, some EM parameters are also a function of the armature current, which has a strong nonlinear character. We use the analytical method (for simplicity, the effect of magnetic circuit saturation is ignored in this paper) instead of the numerical one, mainly because the concept of the analytical method is clear.

A. ELECTROMECHANICAL MODEL

The phase voltage equation of a two-phase motor is similar to that of a rotating three-phase permanent magnet brushless motor, i.e.

$$U_A = R_A i_A + \mathrm{p}\lambda_A \tag{1}$$

$$\lambda_A = L_{AA} i_A + M_{AB} i_B + \lambda_f \sin\theta_e \tag{2}$$

where θ_e is the position angle of mover, expressed as an electrical angle; p is the differential operator $\mathrm{d}/\mathrm{d}t$; U_A is the A axis voltage of the shaft winding; i_A is the stator currents of the A shaft; R_A is A axis stator resistance; λ_A, λ_f are A Shaft stator

and flux linkage, permanent magnet coupling flux linkage, respectively. The meanings of the various inductances in the formula are as follows: L_{AA} and L_{BB} are the self-inductances of the A axis and the B axis, respectively. The mutual inductance between any two windings can be represented by two subscripts M_{AB},the first of which represents the winding that generates the reverse electromagnetic field. The same is true for the B axis, which is omitted here.

A simplified magnetic network model is used and the second and higher harmonic components of the air gap in the periodic permeability are neglected. Based on the definition of inductance and the double-response theory, the self and mutual inductances of the stator A and B phase windings can be derived.

$$\begin{aligned} L_{\mathrm{AA}} &= L_0 - L_2 \cos 2\theta_e \\ L_{\mathrm{BB}} &= L_0 + L_2 \cos 2\theta_e \end{aligned} \tag{3}$$

where L_0 is the constant component of the self-inductance coefficient and L_2 is the amplitude of the second harmonic component of the self-inductance coefficient. When the mover is in segmentation, the mutual inductance is as follows:

$$M_{\mathrm{AB}} = M_{\mathrm{BA}} \approx L_3 + L_4 \sin(2\theta) \tag{4}$$

Where L_3 is the DC component of the mutual inductance and L_4 is the amplitude of the second harmonic of the mutual inductance. The mutual inductance is different when the mover crosses the segment, and the equation is as follows:

$$M_{\mathrm{AB}} = M_{\mathrm{BA}} \approx -L_2 \sin 2\theta_e \tag{5}$$

. Therefore, when considering cross-section operation, the voltage equation is as follows:

$$\begin{aligned} U_{\mathrm{A}} &= i_{\mathrm{A}} R_{\mathrm{A}} + (L_0 - L_2 \cos 2\theta_{\mathrm{e}}) \frac{\mathrm{d}i_{\mathrm{A}}}{\mathrm{d}t} - L_2 \sin 2\theta_e \frac{\mathrm{d}i_{\mathrm{B}}}{\mathrm{d}t} \\ &\quad + 2\, L_2 \left(i_{\mathrm{A}} \sin 2\theta_{\mathrm{e}} - i_{\mathrm{B}} \cos 2\theta_{\mathrm{e}}\right) - k_{\mathrm{e}} \omega_{\mathrm{r}} \sin \theta_e \end{aligned} \tag{6}$$

$$\begin{aligned} U_{\mathrm{B}} &= i_{\mathrm{B}} R_{\mathrm{B}} + (L_0 + L_2 \cos 2\theta_{\mathrm{e}}) \frac{\mathrm{d}i_{\mathrm{B}}}{\mathrm{d}t} - L_2 \sin 2\theta_e \frac{\mathrm{d}i_{\mathrm{A}}}{\mathrm{d}t} \\ &\quad - 2\, L_2 \left(i_{\mathrm{B}} \sin 2\theta_{\mathrm{e}} + i_{\mathrm{A}} \cos 2\theta_{\mathrm{e}}\right) + k_{\mathrm{e}} \omega_{\mathrm{r}} \cos \theta_e \end{aligned} \tag{7}$$

where ω_r is the mechanical angular velocity of rotation, k_{e} is the back-EMF coefficient. At steady state, the armature current can be expressed as follows:

$$\begin{aligned} i_A &= -\hat{i} \sin\left(\frac{\pi}{\tau_p} x + \varphi\right) \\ i_B &= \hat{i} \cos\left(\frac{\pi}{\tau_p} x + \varphi\right) \end{aligned} \tag{8}$$

where $\hat{i}$ is the current amplitude,x is the displacement of the mover, which is converted into an angular signal here.

B. INDUCTION PARAMETERS

During the operation of SW-PMLSM, the degree of coupling between the two-phase winding and the mover is related to the position of the mover [21]. When the mover exists in a certain stator, the permeability of the air gap gradually decreases, and the average value of mutual inductance decreases as the position of the mover increases. Therefore, the expression for the inductance between the parts of the motor can be simplified as:

$$L_k(x) = L_{ok} + L_{km} \cdot \frac{x}{x_n} \tag{9}$$

where: L_{km} is the amplitude of each component of the inductance matrix, L_{ok} is the leakage inductance of the inductance matrix, and when k is taken as 1, 2, 3, 4, $L_1(x)$, $L_2(x)$, $L_3(x)$, $L_4(x)$, $L_(o1)$, $L_(o2)$, $L_(o3)$, $L_(o4)$, $L_(1m)$, $L_(2m)$, $L_(3m)$, $L_(4m)$ is obtained. x_n is the segmented length and x is the effective coupling length. It can be seen that the inductance matrix is a quadratic function of the position, and the effect of the position cannot be eliminated by using rotation coordinate transformation, and the decoupling of dq-axis coordinate system cannot be realized, and the voltage calculation part of the traditional vector control is not accurate.

C. PERMANENT MANGNET COUPLED FLUX

The permanent magnet coupled flux linkage is the function of the permanent magnet to the stator winding of each phase [22]. For SW-PMLSM, when the coupling area between primary and secondary is constant, the coupling magnetic current amplitude of permanent magnets is constant, and the magnitude of permanent magnet coupling magnetic current changes with the change of coupling area between primary and secondary, and when the moving train gradually exits a stator section, the permanent magnet coupling magnetic current linkage gradually decreases to zero, and its change can be regarded as a linear change of approximate analysis. The vector form can be expressed as follows:

$$\psi_{\mathrm{f}}(x) = \psi_{f\,\max} \cdot \frac{x_{\mathrm{s}}}{x_{\mathrm{n}}} \cdot \mathrm{e}^{j\frac{\pi}{\tau}x} \tag{10}$$

where $\psi_{f\,\max}$ is the permanent magnet flux linkage change amplitude, x_n is the segment length, and x_s is the effective coupling length.

D. TRADITIONAL MATHEMATICAL MODEL

The voltage and torque equations of a PMSM d-q model is described as

$$\begin{aligned} U_d &= R_s i_d + \frac{d\psi_d}{dt} - \omega \psi_q \\ U_q &= R_s i_q + \frac{d\psi_q}{dt} + \omega \psi_d \\ T_e &= \frac{3}{2} n_p \left[\psi_f i_q + \left(L_{dd} - L_{qq}\right) i_d i_q\right] \end{aligned} \tag{11}$$

As can be seen from Eq.11, the traditional model treats the motor parameters as constants, ignoring hysteresis losses, core saturation, cross-coupling, eddy current losses, etc. As a result, this simple model inevitably affects the analytical accuracy of WS-PMLSM. In addition, inaccurate motor models can also degrade the dynamic and static performance of the control system. Therefore, it is necessary to reconstruct the WS-PMLSM model to approximate the characteristics of the real motor.

E. STATIONARY COORDINATE SYSTEM MATHEMATICAL MODEL

The permanent magnet linear synchronous motor in $\alpha\beta$ coordinates of the voltage equation can be expressed as:

$$\begin{cases} u_\alpha = R_s i_\alpha + L(x)\dfrac{di_\alpha}{dt} - v\dfrac{\pi}{\tau}\psi_f(x)\sin\theta \\ u_\beta = R_s i_\beta + L(x)\dfrac{di_\beta}{dt} + v\dfrac{\pi}{\tau}\psi_f(x)\cos\theta \\ e_\alpha = -v\dfrac{\pi}{\tau}\psi f(x)\sin\theta \\ e_\beta = v\dfrac{\pi}{\tau}\psi f(x)\cos\theta \end{cases} \tag{12}$$

where: $x = \theta\tau/\pi$ is mover's position, $w = \pi v/\tau$ is electricity angular velocity, e_α and e_β are the back EMF of $\alpha\beta$ axes.

In the two-phase scheme, a current model-based feed-back force estimator is employed. The active and reactive force components are obtained as follows:

$$\begin{aligned} F_a &= \frac{\pi}{\tau_p}\left(\psi_\alpha i_\beta - \psi_\beta i_\alpha\right) \\ F_r &= \frac{\pi}{\tau_p}\left(\psi_\alpha i_\alpha + \psi_\beta i_\beta\right) \end{aligned} \tag{13}$$

in which the armature flux components may be estimated from the motor currents as:

$$\begin{aligned} \psi_\alpha &= L\cdot i_\alpha + \Psi_m \cdot \cos\left(\frac{\pi}{\tau_p}x\right) \\ \psi_\beta &= L\cdot i_\beta + \Psi_m \cdot \sin\left(\frac{\pi}{\tau_p}x\right). \end{aligned} \tag{14}$$

Substituting $\psi_\alpha$and $\psi_\beta$into (18) gives the following force expressions:

$$\begin{aligned} F_a = \frac{\pi}{\tau_p}\Bigg\{\Psi_m\left[i_\beta\cos\left(\frac{\pi}{\tau_p}x\right) - i_\alpha\sin\left(\frac{\pi}{\tau_p}x\right)\right]\Bigg\} \\ + \Psi_m\left[i_\alpha\cos\left(\frac{\pi}{\tau_p}x\right) - i_\beta\sin\left(\frac{\pi}{\tau_p}x\right)\right]\Bigg\} \end{aligned} \tag{15}$$

Compared to the well-known estimators based on the voltage model, the estimator based on the current model has a great advantage because it does not involve the knowledge of the integration operation or the winding resistance. In addition, the winding inductance is small and can be assumed to be constant in position and current. From the direct thrust equation, it can be seen that the thrust is independent of inductance.

II. TWO-PHASE SVPWM ALGORITHM

The basic idea of SVPWM control is to use a certain number of non-zero stationary fundamental vectors in two-dimensional vector space to track and synthesize the spatial rotation vector of the modulating wave, so that the synthesized rotation vector contains as much information of the modulating wave as possible. As an optimized pulse width modulation technique, it has the advantages of cutting harmonics, improving waveform quality to a large extent, increasing the utilization of the DC bus voltage, and being easy to implement digitally using embedded chips such as DSP/ARM.

A. TWO-PHASE INVERTER TOPOLOGY

The control system studied in this paper adopts a two-phase motor. Since it is two-phase, it is not suitable for direct control by a traditional three-phase inverter, so a double H-bridge inverter is used. Its circuit topology is shown in the following Fig.3. It consists of two single-phase H-bridges and a total of eight switches.

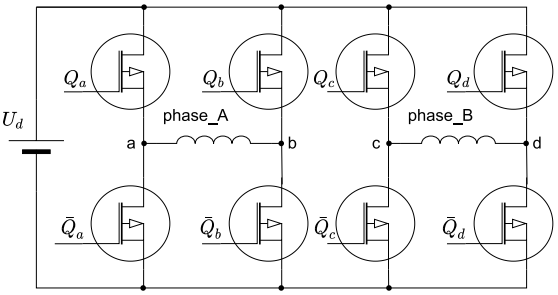

FIGURE 3. Full H-bridge inverter.

A complete H-bridge involves 16 operating states, as twelve active voltage vectors and four zero-voltage vectors are generated, as shown in Figure.4(a).

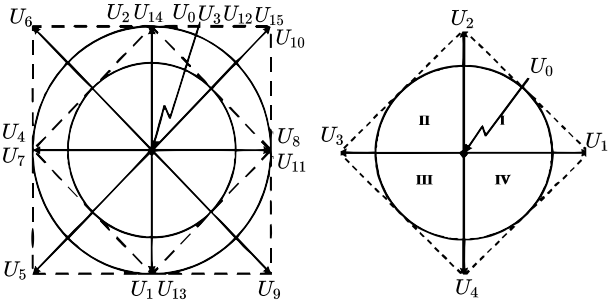

(a)16 basic voltage space vectors (b)4 basic voltage space vectors

FIGURE 4. Voltage space vector diagram.

For simplicity of control, this paper uses diagonal simultaneous conduction, upper and lower complementary conduction, the four non-zero vectors $V_8(1000)$, $V_2(0010)$, $V_4(0100)$, $V_1(0001)$ and one zero vector $V_0(0000)$ are chosen as the basic space voltage vectors, for the convenience of the representation below, they are renumbered as $U_1(1000)$, $U_2(0010)$, $U_3(0100)$, $U_4(0001)$ and $U_0(1000)$. From Fig.4(a), the four selected non-zero fundamental space voltage vectors divide the vector space into four sectors as shown in Fig.4(b), each sector occupies 1/4 of the vector space, and from Table 1, the amplitude of all four non-zero fundamental space voltage vectors is U_d and the phase difference is $\pi/2$.

B. TWO-PHASE SV MODULATION

After coordinate transformation, the components U_α and U_β of the vector U_{ref} in the stationary two-phase orthogonal coordinate system can be obtained as shown in Fig.5

TABLE 1. Double H-bridge inverter basic space voltage vector.

	a	b	c	d	u_A	u_B	$\boldsymbol{u}_s$
$\boldsymbol{V}_0$	0	0	0	0			
$\boldsymbol{V}_3$	0	0	1	1	0	0	0
$\boldsymbol{V}_8$	1	0	0	0			
$\boldsymbol{V}_{11}$	1	0	1	1	U_d	0	U_d
$\boldsymbol{V}_{10}$	1	0	1	0	U_d	U_d	$\sqrt{2}U_d e^{j\frac{\pi}{4}}$
$\boldsymbol{V}_2$	0	0	1	0			
$\boldsymbol{V}_{14}$	1	1	1	0	0	U_d	$U_d e^{j\frac{\pi}{2}}$
$\boldsymbol{V}_6$	0	1	1	0	$-U_d$	U_d	$\sqrt{2}U_d e^{j\frac{3\pi}{4}}$
$\boldsymbol{V}_4$	0	1	0	0			
$\boldsymbol{V}_7$	0	1	1	1	$-U_d$	0	$U_d e^{j\pi}$
$\boldsymbol{V}_5$	0	1	0	1	$-U_d$	$-U_d$	$\sqrt{2}U_d e^{j\frac{\pi}{4}}$
$\boldsymbol{V}_1$	0	0	0	1			
$\boldsymbol{V}_{13}$	1	1	0	1	0	$-U_d$	$U_d e^{j\frac{3\pi}{2}}$
$\boldsymbol{V}_9$	1	0	0	1	U_d	$-U_d$	$\sqrt{2}U_d e^{j\frac{7\pi}{4}}$
$\boldsymbol{V}_{12}$	1	1	0	0			
$\boldsymbol{V}_{16}$	1	1	1	1	0	0	0

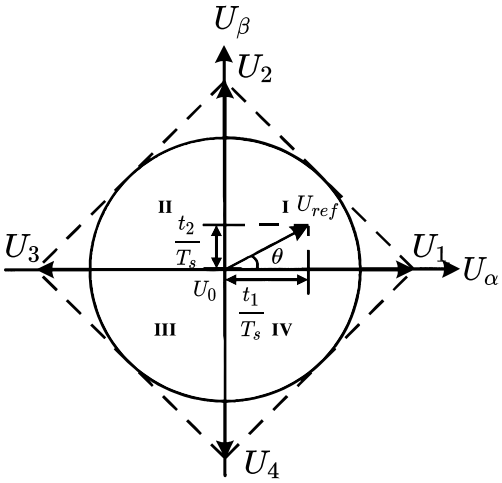

FIGURE 5. Sector distribution in $\alpha\beta$ stationary coordinate.

The sector of the reference vector U_{ref} can be determined from the basic vector distribution: if the voltage reference vector U_{ref} falls in sector I, $U_\alpha > 0$ and $U_\beta > 0$; if the voltage reference vector U_{ref} falls in sector II, $U_\alpha < 0$ and $U_\beta > 0$; if the voltage reference vector U_{ref} falls in sector III, $U_\alpha < 0$ and $U_\beta < 0$; if the voltage reference vector U_{ref} falls in sector IV, $U_\alpha > 0$ and $U_\beta < 0$. It follows that the sector of U_{ref} can be determined by the sign of U_α and U_β. In order to determine the position of U_{ref} in the space sector in a simple way, the following assumptions are made with reference to the method of determining the position of U_{ref} in the space sector of the three-phase vector.

$$A = \begin{cases} 1 & U_\alpha > 0 \\ 0 & U_\alpha \le 0 \end{cases}; \; B = \begin{cases} 1 & U_\beta > 0 \\ 0 & U_\alpha \le 0 \end{cases} \tag{16}$$

Since the different values obtained by the operation of different combinations of the two parameters A and B correspond to the four sectors one by one, define a parameter N,

TABLE 2. N values and sectors.

sector	A	B	N
sector I	1	1	4
sector II	0	1	3
sector III	0	0	1
sector IV	1	0	2

and let

$$N = 1 + A + 2B \tag{17}$$

WhenU_{ref} is in sector I, we can get $U_\alpha > 0$ and $U_\beta > 0$. According to Eq.17, we can get N = 4. Similarly, we can get the one-to-one correspondence between the sector in which U_{ref} is located and the value of N as shown in Table 2. Take the example of sector I where U_{ref} is at this time. As shown in Fig.5, U_{ref} can be synthesized from the non-zero neighboring vectors U_1 and U_2 and the zero vector U_0 at their respective times of action. let Ts be a PWM cycle, and U_{ref} acts equivalently on the non-zero vectors U_1 and U_2 at times t_1 and t_2, respectively, and on the zero vector U_0 at time t_0.From the volt-seconds balance characteristic of spatial voltage vector synthesis, the following equation can be obtained:

$$\int_0^{t_1} \boldsymbol{U}_1 dt + \int_{t_1}^{t_1+t_2} \boldsymbol{U}_2 dt + \int_{t_1+t_2}^{T_s} \boldsymbol{U}_0 dt = \int_0^{T_s} \boldsymbol{U}_{ref} dt \tag{18}$$

Since the carrier frequency is high, make the following simplifications:.

$$\boldsymbol{U}_1 t_1 + \boldsymbol{U}_2 t_2 + \boldsymbol{U}_0 t_0 = \boldsymbol{U}_{ref} T_s \tag{19}$$

where:

$$\begin{aligned} t_0 &= T_s - t_1 - t_2, \quad \boldsymbol{U}_1 = U_d, \; \boldsymbol{U}_2 = U_d e^{j\frac{\pi}{2}} \\ U_0 &= 0, \quad \boldsymbol{U}_{ref} = \left|\boldsymbol{U}_{ref}\right| (\cos\theta + \sin\theta) \end{aligned} \tag{20}$$

Substituting Eq.20 into Eq.19 and simplifying it, we obtain:

$$\begin{aligned} U_d t_1 &= T_s \left|\boldsymbol{U}_{ref}\right| \cos\theta \\ U_d t_2 &= T_s \left|\boldsymbol{U}_{ref}\right| \sin\theta \\ t_0 &= T_s - t_1 - t_2 \end{aligned} \tag{21}$$

Namely:

$$t_1 = \frac{\left|\boldsymbol{U}_{ref}\right| \cos\theta}{U_d} T_s, \quad t_s = \frac{\left|\boldsymbol{U}_{ref}\right| \sin\theta}{U_d} T_s \tag{22}$$

Also:

$$\begin{aligned} U_\alpha &= \left|\boldsymbol{U}_{ref}\right| \cos\theta \\ U_\beta &= \left|\boldsymbol{U}_{ref}\right| \sin\theta \end{aligned} \tag{23}$$

Substituting Eq.23 into Eq.22 yields

$$t_1 = \frac{T_s}{U_d} U_\alpha, \quad t_2 = \frac{T_s}{U_d} U_\beta \tag{24}$$

Similarly, the equivalent action time when U_{ref} is on the adjacent fundamental nonzero vector on the corresponding sector can be found as follows

At sector II:

$$t_1 = \frac{T_s}{U_d} U_\beta, \quad t_2 = -\frac{T_s}{U_d} U_\alpha \tag{25}$$

At sector III:

$$t_1 = -\frac{T_s}{U_d} U_\beta, \quad t_2 = -\frac{T_s}{U_d} U_\alpha \tag{26}$$

At sector IV:

$$t_1 = -\frac{T_s}{U_d} U_\beta, \quad t_2 = \frac{T_s}{U_d} U_\alpha \tag{27}$$

Because the torque current i_q at the output of the speed loop changes greatly in a short time when the motor starts and the load changes suddenly, the amplitude V of the spatial voltage vector at the output of the current loop is likely to exceed the DC bus voltage of the dual H-bridge and over modulation will occur. The spatial voltage vector of the current loop output is constrained within the solid circle shown in Fig.5 and is bounded by the following equation.

$$V = \sqrt{U_\alpha^2 + U_\beta^2} \le \frac{\sqrt{2}}{2} U_d \tag{28}$$

When the qualifying condition is exceeded, the new given voltage vector is:

$$\begin{aligned} U_\alpha^* &= \frac{U_a}{V} \times \frac{\sqrt{2}}{2} U_d \\ U_\beta^* &= \frac{U_\beta}{V} \times \frac{\sqrt{2}}{2} U_d \end{aligned} \tag{29}$$

If we have $t_1 + t_2 > T_s$ without satisfying the constraint, then t_1 and t_2 should become.

$$t_1 = \frac{t_1}{t_1 + t_2} T_s; \quad t_1 = \frac{t_2}{t_1 + t_2} T_s \tag{30}$$

Now let $T_x = \frac{T_s}{U_d} U_\alpha, T_y = \frac{T_s}{U_d} U_\beta$, we can obtain the time t_1 and t_2 relations of U_{ref} acting equivalently on the adjacent base voltage vectors at different sectors as shown in Table 3.

TABLE 3. Time and sector number.

Sectors	I	II	III	IV
N	4	3	1	2
t_1	T_x	T_y	$-T_x$	$-T_y$
t_2	T_y	$-T_x$	$-T_y$	T_x

For this reason, a five-segment SVPWM is used to implement vector modulation, and its waveforms in each sector are shown in Fig.6

III. OPTIMIZING OPERATION OF WS-PMLSM

Due to the structure of the WS-PMLSM, the thrust applied to the mover as it moves through the boundary between the two segments of the WS-PMLSM is the sum of the thrusts provided by the two segments of the motor stator. Therefore, the thrust on the movers as they pass through the junction will

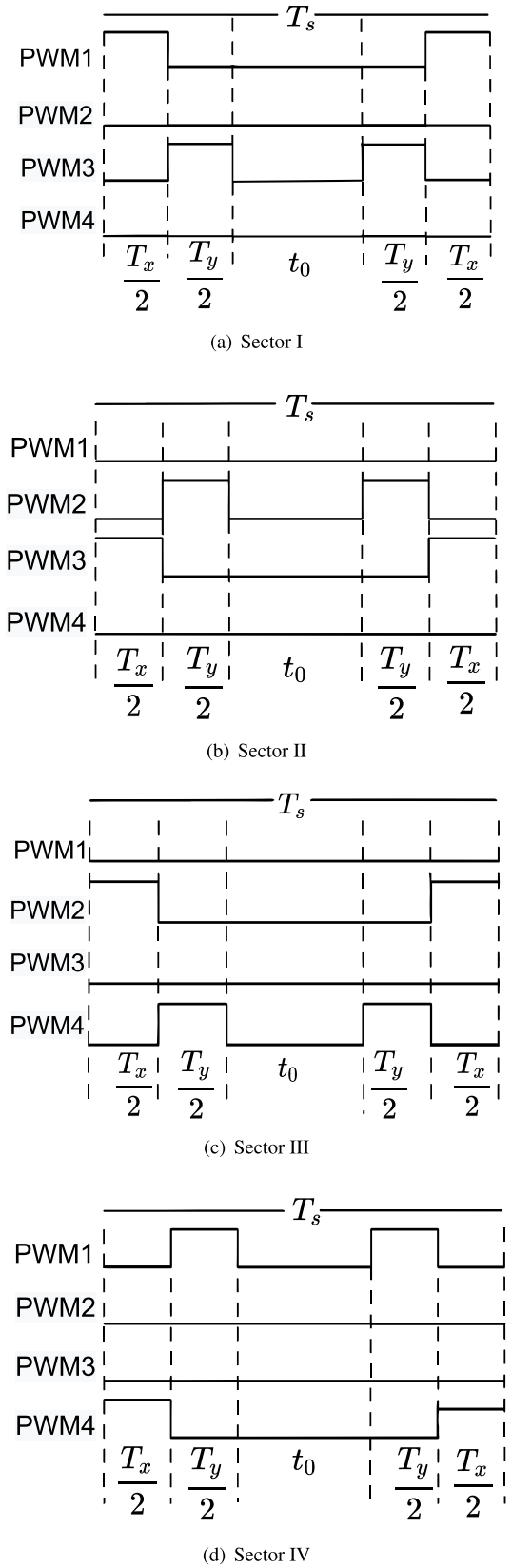

(a) Sector I

(b) Sector II

(c) Sector III

(d) Sector IV

FIGURE 6. Five-segment SVPWM waveform.

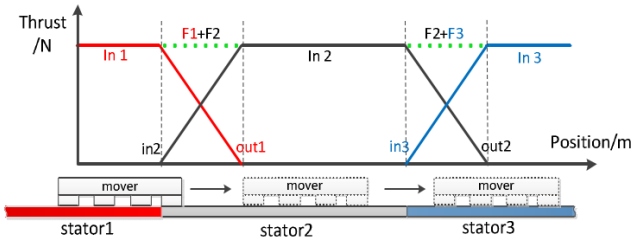

FIGURE 7. Thrust in consideration mover's position [23].

be the same as when they move in the single-segment stator only if the amplitude and phase of the stator currents in the two segments of the motor must satisfy certain mathematical relationships with position, as shown Fig.7.

A. TRADITIONAL METHOD

Conventional strategies can be used to improve the overall performance of segment-based WS-PMLSM systems. These strategies include coordinating the drive of the separator [23], compensating for different field array coverage [24], and optimizing the efficiency by running different currents in each stator (three-phase winding) [25]. The following is a brief description of this approach, which strictly guarantees the synchronization of the phase currents of the two stator sections of the motor in dq coordinates

$$\begin{aligned} F_e &= F_{e1} + F_{e2} \\ &= \frac{3\pi}{2\tau} p \left(\psi_{f\_\text{out}}(x) + \psi_{f\_in}(x)\right) i_q \\ &= \frac{3\pi}{2\tau} p \psi_f(x) i_q \end{aligned} \tag{31}$$

where: $i_q = i_{q1} = i_{q2}$ is the q-axis current of the two segments. However, due to the structure of each stator segment and the different degree of coupling between the motor and the master and slave stator segments, the dynamic response of each controller is also different, resulting in certain errors and delays between the actual currents of the two stator segments and the currents given by the system, which leads to large differences and delays in the relative current values of the two stator segments, resulting in inconsistent electromagnetic thrust and excitation generated by the two stator segments of the motor.

B. OPTIMAL METHOD

In contrast to the above, further optimal control can be achieved by driving different currents in each stator depending on the coverage of the stator by the magnetic field array, e.g., the magnetic field array completely covers one stator but overlaps only slightly with the second stator. If the currents in both stators are equal, then the forces on the second stator are small, but the resulting resistance losses are also equal. By driving the first stator but not the second, the same force can be obtained while consuming less total power. References [25], [26]. Several cases are discussed below

1) EMF-BASED FEEDFORWARD

It is often desirable to add feedforward terms to the current control loop to improve transient performance [27]. Since the resistance, inductance and counter-electromotive force constants of the motor are usually known, their effects can be compensated for in the current control loop. The back-EMF constants of the WS-PMLSM stator vary with position, since the permanent magnetic field array may not be completely covered by the stator. The electromagnetic field of the motor is proportional to the speed and is approximately proportional to the extent to which the stator is covered by the magnetic field array. The stator coverage factor C_k can be calculated as the percentage of the stator that is covered by the magnet array:

$$C_k = \frac{x_\text{k}}{x_\text{n}} \tag{32}$$

where x_n is the segment length, and x_k is the effective coupling length of segment k. Thus, the back-EMF for a particular stator may be computed from the motor constant K_t, the frequency ω, and the stator coverage C_k

$$V_\text{EMF} = K_t \cdot \omega \cdot C_k \tag{33}$$

In the steady-state vector-controlled case, the current I is equal to the real-valued desired current I_q. the feedforward voltage can be written as:

$$\mathbf{V}_{FF} = (j\omega L + R) I_q + V_\text{EMF} \tag{34}$$

The block diagram of the above formula implementation is as Fig.8

2) EFFICIENCY OPTIMIZATION

The WS-PMLSM stator is usually divided into smaller modules. This approach improves the efficiency of the drive system because the resistance losses in the unenergized part are eliminated and it also reduces the heat generated by the stator. The power dissipation to be minimized can be expressed as follows:

$$P = \sum_{k=1}^{m} I_k^2 R_k \tag{35}$$

I_k, R_k are the equivalent currents and resistances of each stator section. In order to establish the force constraint in the function to be minimized, the process can be controlled using the principle of minimizing the stator current vector amplitude according to the model reconstruction Lagrangian operator, i.e., the minimum current to achieve the desired thrust.

$$\begin{aligned} M &= P + \rho \left(F^* - F\right) \\ F &= \sum_{k=1}^{m} C_k K_k I_k \end{aligned} \tag{36}$$

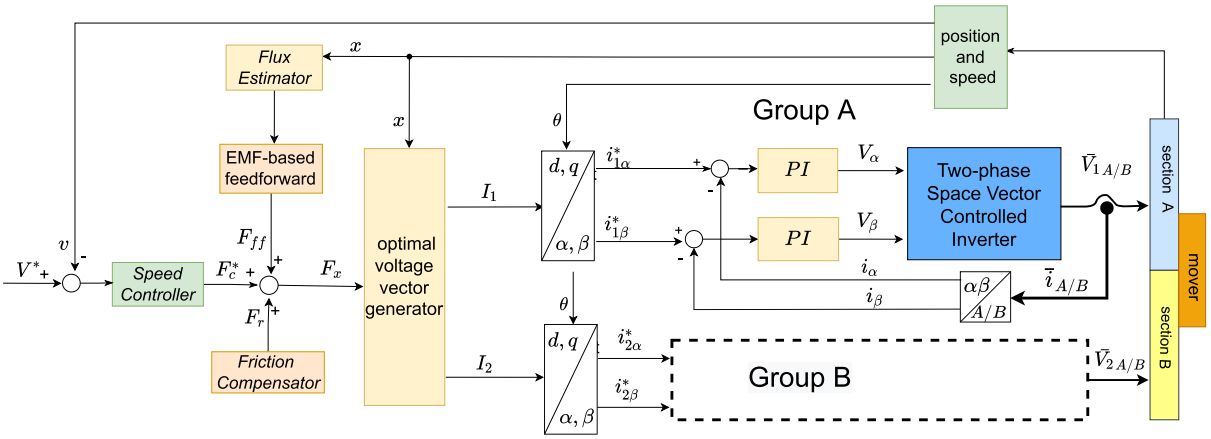

FIGURE 8. Experimental prototype of the proposed system.

The following conditions need to be met.

$$\begin{cases} \dfrac{dM}{dI_k} = 0 \\ \dfrac{dM}{d\rho} = 0 \end{cases} \tag{37}$$

we obtain current commands, such that

$$I_n = \rho\left(\frac{K_n C_n}{2R_n}\right) \tag{38}$$

$$\rho = \frac{F}{\sum_{k=1}^{m} \frac{C_k^2 K_k^2}{2R_k}} \tag{39}$$

It is now possible to solve directly for the optimal currents

$$I_n = F\frac{C_n K_n}{R_n \sum_{k=1}^{m} \frac{C_k^2 K_k^2}{R_k}} \tag{40}$$

the current $I_n$is equal to the real-valued desired current I_q. For example, if only two segments are considered, with equal resistance and motor coefficients, the following segment currents are obtained:

$$\begin{aligned} I_1 &= F\frac{C_1}{C_1^2 K_1 + C_2^2 K_1} \\ I_2 &= F\frac{C_2}{C_1^2 K_1 + C_2^2 K_1} \end{aligned} \tag{41}$$

IV. EXPERIMENTAL SETUP

Fig. 9 shows the structure of a two-phase segmented-winding linear propulsion motor. The motor consists of a segmented stator and a passive mover, the stator comprising an iron core, a coil winding and a stator tooth slot. The two-phase coil A and B windings are wound at equal intervals on the stator tooth slot with an electrical angle of 90^0, and the mover consists of a permanent magnet and an iron core.

The parameters of PMLSM are given in Table 4 for the fabrication of a passive carrier with a width of 150mm and a stator with a length of 1000mm. The stator is composed of 10 sets of two-phase winding modules. The passive carrier

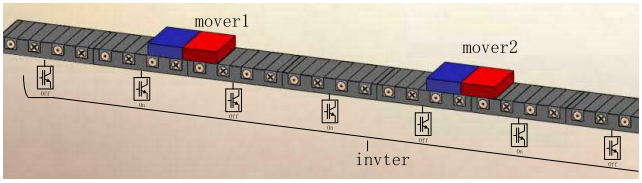

FIGURE 9. Structure and control of the WS-PMLSM.

TABLE 4. Parameter of WS-PMLSM.

Description	Symbol	Value	Unit
Length of segmented stator	2τ	100	mm
Pitch of permanent magnet	τ	50	mm
Pitch of coil	τ_c	50	mm
Turn of coil	n	10	$turns/slot$
Resistance of coil	R	2.553	ohm/phase
Inductance of coil	L	17	mH/phase
Number of poles	$number$	2,3	any combination
Connection pattern	$node$	star/tri	any combination
Stator marerials			50JN470
Magnet marerials			NEOMAX-35SH
Magnet residual magnetic	B_r/T	1.16	T
Magnet coercive force	H_{cj}	1671	KA/m^{-1}
Mover yoke marerials			50JN470

is supported by a linear bearing consisting of LM tracks. The passive carrier at the origin of the permanent magnet is measured by a non-contact linear encoder.

Fig. 10 shows the current amplifier, the excitation circuit and the thrust controller module used in the experiment. The current amplifier is implemented by a PWM controller that uses a MOSFET power switching device with a drive voltage of $24V$. Since driving a non-effective coil can cause false thrust currents and interfere with thrust, a power MOSFET with zero-current shutdown was used to switch the coil. The carrier propulsion controller uses an STM32G474 as the CPU. in order to operate a module, a total of two STM32G474s are required. each CPU controls six coils, and the remaining one is used to wait for the next module to switch. 10 stator coils are connected to the CPU through

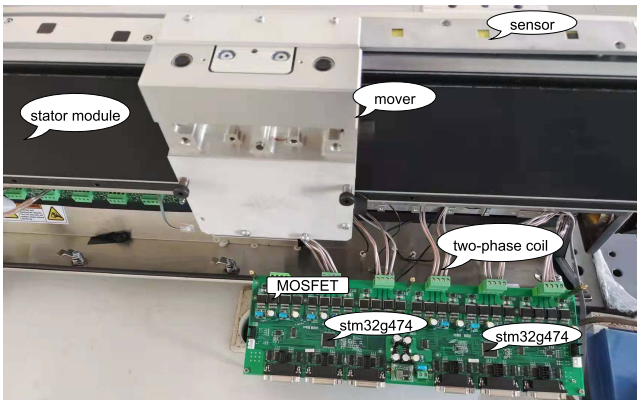

FIGURE 10. Experimental prototype of the proposed system.

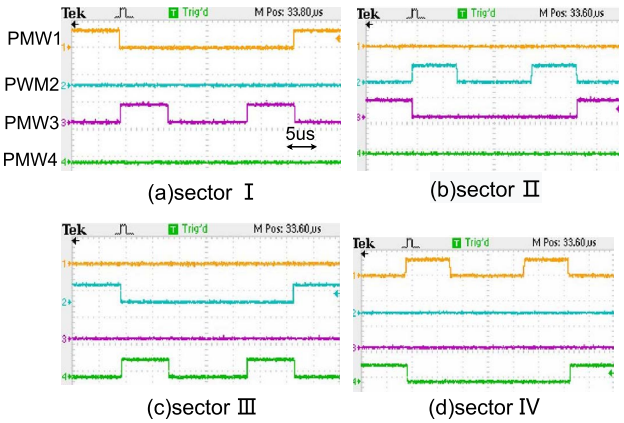

FIGURE 11. Waveform of five-segment SVPWM.

a reward circuit. The reward circuit determines the number of coils to be connected based on the carrier's motion and vector characteristics.

V. EXPERIMENT AND ANALYSIS

A. TWO-PHASE INVERTER

In this section, the proposed SVPWM control strategy as well as the control algorithm are experimentally tested. The experimental results are presented one by one in the following.

1) SVPWM MODULE WAVEFORM VERIFICATION

The software implementation of SVPWM on ARM using the enhanced pulse width modulation module shows that the waveform of SVPWM implemented in software basically matches that of the vector modulation method designed in this paper (Fig.6) as shown in Fig.11, Only the waveform marker of sector 1 is marked in the figure, the other three sectors are the same as the sector, and the time frame of the oscilloscope is 5us,the voltage frame is 5v.

2) SVPWM TWO-PHASE CURRENT WAVEFORM

Given motor speeds of 0.1m/s and 0.4m/s, the motor two-phase winding current waveforms obtained in the experiment are shown in Fig.12.The observation shows that the

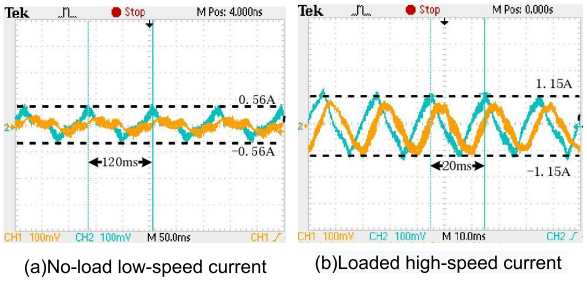

FIGURE 12. Two-phase current waveform.

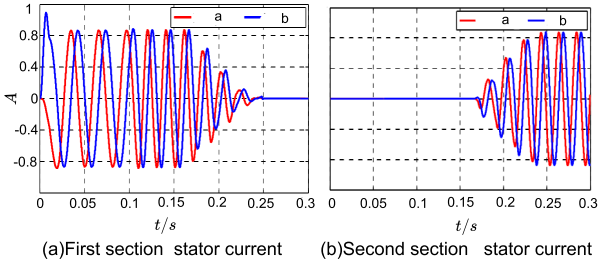

FIGURE 13. Inter-segment transition current.

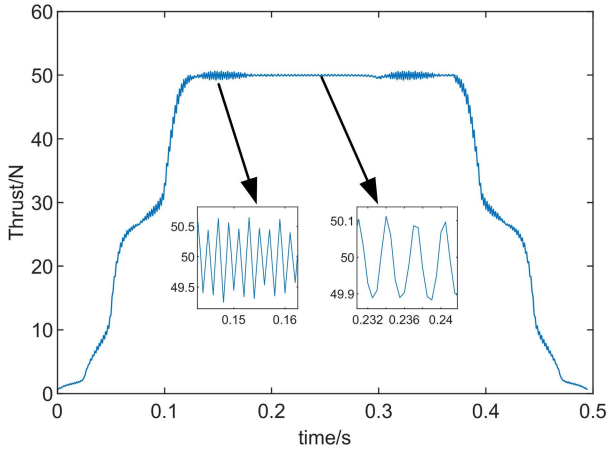

FIGURE 14. Change thrust of the movers.

current waveform is not ideal when the motor is at light load and low speed, but at a certain load or speed, the current waveform is close to ideal.

Fig.13 shows the current variation process in the two parts of the stator, where the mover runs between the two parts. As the mover gradually moves out of the first stator, the amplitude of the current decreases, related to the degree of decay of the coupling area, until it decreases to zero after moving out completely. As the mover moves into the second stator, the amplitude of the current gradually increases, proportional to the change in the coupling area.

B. FORCE CONTROL OF TWO-PHASE MOTOR

Fig.14 shows the variation of the thrust force during the operation of the mover. When the mover gradually enters the

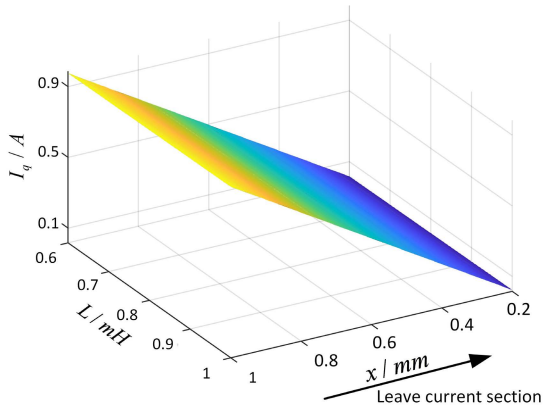

FIGURE 15. Transition current leaving the current section.

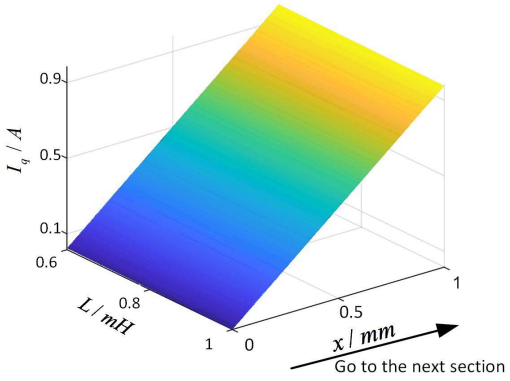

FIGURE 16. Transition current going to the next section.

excitation magnetic field generated by the stator winding, the magnitude of the thrust on the mover gradually increases, and the thrust on the mover fluctuates greatly under the action of the end; when the mover are fully coupled with the stator winding, the magnitude of the thrust is basically stable at about 50N; when the mover leave the stator winding, the thrust on the mover decreases rapidly and finally drops to zero.

The transition curve in Fig.14 is approximately composed of a quadratic curve and segmented linearity, which basically matches the optimal thrust curve analyzed above. two local enlargements in Fig.14 show the fluctuation of the thrust force, which is caused by the tooth groove effect and is not discussed here, and can be seen to have a relatively small amplitude.

Fig.15 shows the relationship between inductance, position and current. It can be seen from the figure that the inductance has a relatively small effect on the current, while revealing the change in the current command as the mover gradually leaves the current section, i.e., the current gradually decreases as the coupling area decreases.

Fig.16 shows the opposite motion to Fig.reffig14, i.e. the thrust current response of the now stator as the mover progressively moves into the next section of the stator. The two are very complementary to each other and the effect of the transition inductance is relatively small.

VI. CONCLUSION

In this paper, we present a preliminary study of the now more promising WS-PMLSM. Since the mathematical model of WS-PMLSM has surpassed various motor assumptions nowadays, there are relatively few related research literatures. Therefore, we first analyzed the relevant parameters of the WS-PMLSM mathematical model. These analytical procedures can provide an effective reference for future advanced control, and we finally choose a two-phase motor model to design WS-PMLSM in which the intermediate complex mathematical calculations are simplified. Second, we propose an adaptation of the two-phase SVM technique in order to apply it to the control scheme of the two-phase WS-PMLSM prototype. Although direct thrust control (DTC) is a popular research topic, we do not use this technique considering the smoothness of operation.

Another important difficulty of WS-PMLSM is the cross-sectional operation of the mover. When two stators drive a mover together, there is very little literature on how these two stator currents are distributed. The traditional approach is to use two stator currents of the same amplitude and phase, but this will affect the efficiency and covering less stator heating is unavoidable. To solve this problem, this paper uses Lagrange operators and proposes an optimization algorithm to achieve better results in a two-phase motor.

The next plan is to design a high-performance virtual SVM or DTC to virtualize the two stator sections of the transition process into one stator section.

REFERENCES

[1] M. Mihalachi, R. Leidhold, and P. Mutschler, "Motion control for long primary linear drives used in material handling," in *Proc. 14th Int. Power Electron. Motion Control Conf.*, 2010, pp. T5-94–T5-101.
[2] T. Zhang, X. Mei, and X. Du, "Absolute position acquisition for linear synchronous motor with passive mover," *IEEE Access*, vol. 9, pp. 100757–100768, 2021.
[3] L. Huang, Y. Chen, H. Kong, Q. Lu, and Y. Ye, "Analysis of a permanent magnet linear synchronous motor with segmented armature for transportation system," in *Proc. 17th Int. Conf. Electr. Mach. Syst. (ICEMS)*, Oct. 2014, pp. 1791–1796.
[4] C. R. Lines, "Modelling and control of segmented long-stator permanent-magnet linear synchronous motors," Ph.D. dissertation, Dept. Eng. Built Environ., Univ. Witwatersrand, Johannesburg, South Africa, 2014.
[5] M. Wang, L. Li, D. Pan, Y. Tang, and Q. Guo, "High-bandwidth and strong robust current regulation for PMLSM drives considering thrust ripple," *IEEE Trans. Power Electron.*, vol. 31, no. 9, pp. 6646–6657, Sep. 2016.
[6] L. Li, H. Zhu, and C. C. Chan, "Investigation of the inter-stator current control for long primary winding segmented PMLSM used in electromagnetic launch system," in *Proc. 17th Int. Symp. Electromagn. Launch Technol.*, Jul. 2014, pp. 1–6.
[7] M. Ma, L. Li, Z. He, and C. C. Chan, "Influence of longitudinal end effects on electromagnetic performance of an permanent magnet slotless linear launcher," in *Proc. 16th Int. Symp. Electromagn. Launch Technol.*, May 2012, pp. 1–6.
[8] K.-C. Lee, M.-T. Kim, and E.-H. Song, "New design of a permanent magnet linear synchronous motor for seamless movement of multiple passive carriers," *Trans. Korean Inst. Power Electron.*, vol. 20, no. 5, pp. 456–463, Oct. 2015.
[9] M. A. Mihalachi, "Position acquisition and control for linear direct drives with passive vehicles," Ph.D. dissertation, Technische Universität, Darmstadt, Germany, 2011.
[10] J. Hong, L. Li, Z. Zong, and Z. Liu, "Current error vector based prediction control of the section winding permanent magnet linear synchronous motor," *Energy Convers. Manage.*, vol. 52, no. 11, pp. 3347–3355, Oct. 2011.

[11] M. Mihalachi and P. Mutschler, "Capacitive sensors for position acquisition of linear drives with passive vehicles," in *Proc. 12th Int. Conf. Optim. Elect. Electron. Equip.*, 2010, pp. 673–680.
[12] V. Kremer, Z. Q. Zhu, and D. Howe, "Indirect and direct force control of a two-phase tubular permanent magnet machine," *IEEE Trans. Power Electron.*, vol. 22, no. 2, pp. 654–662, Mar. 2007.
[13] L. Quéval and H. Ohsaki, "Nonlinear abc-model for electrical machines using N-D lookup tables," *IEEE Trans. Energy Convers.*, vol. 30, no. 1, pp. 316–322, Mar. 2015.
[14] T. Zhang, X. Du, and X. Mei, "Modelling and analysis of two-phase winding segmented permanent magnet linear synchronous motor," in *Proc. 13th Int. Symp. Linear Drives Ind. Appl.*, pp. 1–6, 2021.
[15] I. C. Gros, M. Radulescu, C. Marginean, and T. Petre, "Electromagnetic and dynamic performance analysis of a two-phase permanent-magnet tubular linear actuator," *Acta Electrotehnica*, vol. 56, no. 4, 2015.
[16] Q. Wang, K. Wang, M. Zhao, Y. Zheng, X. Cao, and B. Zhang, "Research on sensorless control for long-stator linear synchronous motors applied in maglev trains under the influence of levitation system," in *Proc. 13th Int. Symp. Linear Drives Ind. Appl.*, 2021, pp. 1–4.
[17] A. Zahid, F. Khan, N. Ahmad, I. Sami, W. Ullah, N. Ullah, N. Ullah, and H. I. Alkhammash, "Design and analysis of dual mover multi-tooth permanent magnet flux switching machine for ropeless elevator applications," *Actuators*, vol. 10, no. 4, p. 81, Apr. 2021.
[18] Q. Lu, B. Wu, Y. Yao, Y. Shen, and Q. Jiang, "Analytical model of permanent magnet linear synchronous machines considering end effect and slotting effect," *IEEE Trans. Energy Convers.*, vol. 35, no. 1, pp. 139–148, Mar. 2020.
[19] L. Cui, H. Zhang, and D. Jiang, "Research on high efficiency V/f control of segment winding permanent magnet linear synchronous motor," *IEEE Access*, vol. 7, pp. 138904–138914, 2019.
[20] L. Xu and Z. Q. Zhu, "A novel SVPWM strategy for open-winding machine with low current ripples," in *Proc. IEEE Int. Electric Mach. Drives Conf. (IEMDC)*, May 2021, pp. 1–7.
[21] L. Liyi, J. Hong, Z. Lu, L. Ying, Y. Song, L. Rizhong, and L. Xiaopeng, "Fields and inductances of the sectioned permanent-magnet synchronous linear machine used in the EMALS," *IEEE Trans. Plasma Sci.*, vol. 39, no. 1, pp. 87–93, Jan. 2011.
[22] R. B. Oswald, "Investigation of control methods for segmented long stator linear drives," Ph.D. dissertation, Technische Universität, Darmstadt, Germany, 2008.
[23] L. Li, H. Zhu, M. Ma, and Q. Chen, "Proposal of the sensorless control method of long primary segmented PMLSM applied in electromagnetic catapult," in *Proc. 16th Int. Symp. Electromagn. Launch Technol.*, May 2012, pp. 1–4.
[24] R. Benavides and P. Mutschler, "Compensation of disturbances in segmented long stator linear drives using finite element models," in *Proc. IEEE Int. Symp. Ind. Electron.*, pp. 2445–2449, Jul. 2006.
[25] B. Perreault, "Optimizing operation of segmented stator linear synchronous motors," *Proc. IEEE*, vol. 97, no. 11, pp. 1777–1785, Oct. 2009.
[26] B.-G. Gu and K. Nam, "A vector control scheme for a PM linear synchronous motor in extended region," *IEEE Trans. Ind. Appl.*, vol. 39, no. 5, pp. 1280–1286, Sep. 2003.
[27] F. Xie, W. Hong, and C. Qiu, "Speed fluctuation suppression of PMSM using active disturbance rejection and feedback compensation control," *IET Electr. Power Appl.*, vol. 15, no. 4, Mar. 2021.

TUANSHAN ZHANG received the B.S. degree from Xi'an Polytechnic University, Xi'an, China, in 2005, and the Ph.D. degree in electric drive transportation with the Mechanical Engineering Department, Xi'an Jiaotong University, Xi'an, in 2020.

He is currently an Associate Professor with the Mechanical and Electrical Engineering Department, Xi'an Polytechnic University. He has conducted extensive research and authored more than 40 peer-reviewed papers. He holds ten patents. His research interests include design, modeling, control of battery systems, electric vehicles, renewable energy systems, and robots.

XUESONG MEI received the Ph.D. degree in mechanical engineering from Xi'an Jiaotong University, Xi'an, China, in 1991.

He is currently a Full Professor with the School of Mechanical Engineering and the Director of the Shaanxi Key Laboratory of Intelligent Robots, Xi'an Jiaotong University. His research interests include intelligent manufacturing, robotics, and precision laser processing.

XIN DU was born in Shanxi, China, in 1996. He received the B.S. degree in mechanical design manufacture and automation from Shanxi Agricultural University, China, in 2019. He is currently pursuing the M.S. degree in mechanical engineering with Xi'an Polytechnic University, Xi'an, China. His research interest includes design and control of linear motors.